

Solution-Processed LiF for Tailoring the Work Function in Electrode Bilayers

Taner Aytun,[†] Ayse Turak,[‡] Iain Baikie,[§] Grzegorz Halek,[§] and Cleva W. Ow-Yang^{†,}*

[†]Sabanci University, Materials Science & Engineering Program, Istanbul, 34956, Turkey

[‡]Max Planck Institute for Metals Research, Department of Low Dimensional and Metastable
Materials, Heisenbergstrasse 3, Stuttgart, D-70569, Germany

[§]KP Technology, Ltd., Burn Street, Wick, Caithness KW1 5EH, Scotland, United Kingdom

CORRESPONDING AUTHOR:

*E-mail: cleva@sabanciuniv.edu

**RECEIVED DATE (to be automatically inserted after your manuscript is accepted if
required according to the journal that you are submitting your paper to)**

Although ambient processing is the key to low-cost organic solar cell production, high-vacuum thermal evaporation of LiF is often a limiting step, motivating the exploration of solution processing of LiF as an alternative electrode interlayer. Sub-monolayer films are realized with the assistance of polymeric micelle reactors that enable LiF particle deposition with controlled nanoscale surface coverage. Scanning Kelvin probe reveals a work function

tunable with nanoparticle coverage, with higher values than that of bare tin-doped indium oxide.

KEYWORDS: surface work function tuning, Kelvin probe, organic solar cells, LiF, depolarization

One of the primary advantages of organic electronics, such as solar cells, is the potential for low-cost mass production of large-area devices.¹⁻⁵ While fully vacuum deposited OLEDs have already been introduced into the marketplace, solution-based polymer devices have not been able to effectively take advantage of ambient processing, due to the need for costly and time-consuming vacuum deposition of inorganic electrodes.¹⁻⁴ As the current state-of-the-art organic solar cells are based on solution-processed polymer blends,⁶ introducing non-vacuum techniques for electrode fabrication remains an essential step in realizing fully ambient manufacturing of devices. Recently, an inverted device structure deposited entirely from solution was realized by Krebs and co-workers for roll-to-roll manufacturing.¹⁻⁴ This achievement demonstrates the feasibility of complete ambient processing, consequently inspiring the development of more suitable materials systems.

Though a wide variety of interlayers have been attempted in organic devices, LiF has seen widespread use at both high work function⁷⁻⁹ and low work function¹⁰⁻¹² electrodes, due to the dramatic enhancement of electrode properties. Despite the fact that the exact mechanism is still controversial, LiF is known to mainly affect the electrode surface work function (Φ), which plays a central role in determining the efficiency and performance of a device.¹³⁻¹⁶ While other solution processed interlayers have been realized, including most recently CsF¹⁷ and ZnO nanoparticles,¹⁻⁴ the incorporation of LiF to date still necessitates high-vacuum techniques, due to the poor solubility of LiF. However, the versatility of LiF for use at both

electrodes makes a compelling case for the development of a solution-processed route for LiF, for the eventual use with an appropriate solution processed electrode at the top-side contact.

Electrode work function (Φ) plays a major role in the performance of devices, as adjustment of Φ results in changes of the interfacial energy level alignment with the active organic layer and changes in carrier tunneling probability.^{7,13} Modification of the surface has led to both positive and negative changes in Φ , depending on the treatment. Thermally evaporated LiF has been observed to decrease the Φ of metallic electrodes;^{13,18} plasma etching has led to increases in Φ of indium tin oxide (ITO);¹⁹ while self-assembled monolayers can induce surface dipole change in either direction, by employing lateral depolarization effects.²⁰

Specifically, to reduce the energy barrier at the anode, modification of the ITO surface is based on increasing Φ , by passivation with surface-active species²¹ or by chemical and physical treatments.^{14,19,22} The possibility of tailoring the work function to match the energy level of the active organic layer is of great interest in the fabrication of organic devices to form barrier-free Ohmic contacts, where the work function no longer controls device performance.

The goal of this letter is to demonstrate the viability and the added benefit of work function tunability of a solution-processed route to the growth of LiF. To synthesize LiF particles in solution, diblock copolymer (BCP) reverse micelles are used as reactor vessels to control the nanoscale size, shape and polydispersity of the particles produced.^{23,24}

We have produced an electrode bilayer consisting of solution-processed LiF (sol-LiF) deposited onto ITO and examined the work function using scanning Kelvin probe (SKP). The average value of an entire surface can be obtained by SKP measurement rastered at the macroscale. As device performance is a global value, made up of averaging in parallel all of the local “cells” that arise from microscopic differences on the electrode surface, SKP analysis is ideally suited for probing the impact of interlayers in devices.¹⁵ To control the

degree of sub-monolayer coverage of the ITO substrate, the number of successive LiF deposited was varied to demonstrate engineering of the surface work function.

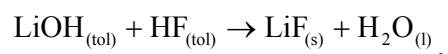
For LiF particle synthesis in solution, polystyrene-*block*-poly 2-vinylpyridine (PS-*b*-P2VP) diblock copolymer (BCP) (Polymer Source, P1330-S2VP) was dissolved in toluene.²⁵ After confirming the formation of spherical reverse micelles by dynamic light scattering, non-hydrated lithium hydroxide (LiOH) and hydrofluoric acid (40% buffered, technical grade) were added sequentially. DLS was also used to verify reactant loading to the micelle core (see Supporting Information, Figure S1).

To validate formation and contrast the influence of the micelles reactors on LiF formation, LiF synthesized in solution with and without micelles was analyzed by scanning electron microscope imaging, X-ray photoelectron spectroscopy, and diffraction.²⁵

To control the sub-monolayer arrangement and increasing density of LiF particles, the procedure depicted schematically in Figure 1(a) was followed. A monolayer of LiF-loaded micelles was deposited onto ITO-coated glass substrates by spin-coating the micelle solution. Oxygen plasma etching (PVA Tepla America Inc. and Harrick PDC-002) was used to remove the polymeric micelles,²⁶ revealing an array of LiF particles.²⁵ The bare ITO-coated glass substrates were also subjected to the same etching conditions.

The work function of exposed LiF (processed in micelles) was compared with that of thermal evaporated LiF²⁵ by scanning Kelvin probe measurements.^{25,27} SKP reveals the average Φ underneath the rastered tip.

Without the micelles, the combination of LiOH and HF in toluene,



yields cubes of ionic crystalline LiF of a broad size polydispersity (see Figure 1d), as also demonstrated previously by Sarraf-Mamoory and co-workers.²⁸ Using reverse BCP micelles

not only enabled a monodisperse size distribution (see Supplementary Information), but also facilitated the deposition of a single layer LiF particles with a surface coverage of $\sim 14.1\%$, as shown in the secondary electron image in Figure 1*b*. Successive coating and etching steps led to sequentially increasing coverage of the substrate surface by mostly disconnected LiF islands (see Figure 1*c*). According to SEM measurements of 547 particles, the reverse micelle synthesis produced roughly spherical islands of 16.6 ± 6.0 nm, on average. Thermal evaporation of LiF to a nominal 0.5-nm thickness, measured by quartz crystal monitor, onto ITO substrates led to the formation of connected flat nanoparticle islands with sub-monolayer coverage, with a characteristic island size of ~ 40 nm that was confirmed by atomic force microscopy imaging (see Supplementary Information). The thickness at which an evaporated LiF interlayer effectively improves device performance is limited to ~ 1 nm in both OLEDs and OPVs.^{12,16} Above such thicknesses, complete coverage of the ITO surface by crystalline LiF was observed.

Figure 2 summarizes the diffraction data obtained from the loaded micelles. Both X-ray and electron diffraction spectra can be indexed to LiF, with (111) and (200) peaks at $q_z \approx 2.7$ and 3.1 \AA^{-1} , proving that powder-like crystalline LiF particles had indeed formed inside the polymeric micelle core. It should be noted that similar measurements of unloaded micelles, or ones loaded only with LiOH, showed none of these characteristic signatures of LiF formation.

To confirm the formation of ionic LiF, the LiF synthesized in solution was characterized by XPS. All spectra were aligned using adventitious C at the surface, at 284.8 eV.²⁹ Figure 3 shows the core level binding energy peaks of the solution-processed LiF, produced both with and without the micelles, in comparison to thermally evaporated LiF. Table 1 outlines the binding energies and concentration ratios for the three types of LiF.

The LiF processed in solution without micelles and the thermally evaporated LiF both show the characteristic Li-1*s* at 55.3 eV and F-1*s* binding energy peak at 685 eV, consistent with those of ionic LiF.²⁹ Assignment of the high binding energy feature on the F-1*s* is currently

under investigation, but the spectral feature appears to be a signature of solution-processed LiF. Note that the micelle-reactor LiF shows both characteristic features of solution-processed LiF in the F-1s core level. However, for the etched particles from the micelles, a shift of 1.4 eV is observed. A majority of that shift, 1.1eV, can be attributed to the non-uniform charging of the surface due to the presence of nanoscale objects,³⁰ also observed for the Li-1s. The remaining shift to a slightly higher binding energy of F-1s ($\Delta=0.3\text{eV}$), compared to thermally evaporated LiF, may be attributed to a charge transfer interaction between LiF and the ITO surface, with received charge from the substrate. A second possibility is a size-related shift, observed in both metal and compound nanoparticles/nanosolids,³¹⁻³³ arising from the increased surface area of the nanoscale islands. Both possibilities would support the formation of a dipole at the nanoparticle surface. The value of the chemical shift is not consistent with known possible compounds of fluorine in this environment.²⁹

The surface averaged Φ values from SKP for various samples are summarized in Table 2 for solution-processed LiF forming an electrode bilayer with ITO (sol-LiF/ITO) and for thermal evaporated LiF on ITO (thermo-LiF/ITO). As exposing the LiF particles for subsequent device processing steps necessitated an O₂ plasma etch, the effect of plasma treatment on Φ was also evaluated on bare ITO and thermo-LiF/ITO. As the average macroscopic work function is of interest for assessing electrode bilayer performance, a 2-mm diameter probe head was used. The micro- and nanoscale variations inherently present in the surface topography of the ITO surface^{15,34} were very similar before and after deposition of the ultra-thin LiF films, all of which consist of nanoparticle islands. This indicates that the LiF had a uniform impact on the ITO surface in all cases.

The standard deviation about the average work function for all samples ranged over 20-60 meV, which is consistent with the macroscopic work function measurements on real surfaces, *i.e.* surfaces that contain modest inhomogeneity, such as scratches, justifying the averaging of

the surface work function. In fact, if a 20x20 mm section of a pristine Au reference sample is scanned with a 2-mm tip, then the mean work function will be 4-6 meV. The values reported in Table 2 correspond to the mean work function across a whole scan area. To emphasize the impact of the various forms of LiF on the ITO surface, Table 2 also shows the relative change in the electrode work function, referenced to that of the as-received, bare ITO.

Evaporation of LiF onto ITO (thermo-LiF) led to a reduction in the Φ of ITO (see Table 2), consistent with observations on metal surfaces,^{13,18} as well as with the reduction recently reported for LiF on ITO by UPS.³⁵ To compare the effect of the O₂ plasma etch process on the surface of LiF, the Φ of as-deposited thermo-LiF was compared with the Φ of the thermo-LiF layer subjected to the same O₂ plasma etch process as was used to remove the micelles for the sol-LiF layers. For direct comparison with bare ITO, the ITO substrate was masked during thermal evaporation of LiF, in order to produce regions of LiF-covered and bare ITO simultaneously. The measurements (see Table 2) show that $\Delta\Phi$ resulting from plasma etching was the same in magnitude and direction for both the bare (as-received) ITO and the 0.5 nm-thick thermo-LiF ($\Delta\Phi_{0.5\text{nm,LiF}} = 0.14$ eV). As the substrates were partially masked during LiF deposition, the values described are a direct comparison of etching of bare and covered ITO simultaneously. Typically, an increase in Φ is associated with the oxidation of the ITO surface and absorption of OH species.^{15,22} AFM revealed that the 0.5 nm-thick thermo-LiF layer also consists of sub-monolayer coverage, with ~40-nm diameter islands, *i.e.* some underlying ITO is exposed during etching. Thus the increase in Φ is most likely due to oxidation of ITO, with little effect of O₂ plasma etching on the surface properties of thermo-LiF. Similarly, the presence of LiF islands does not appear to change the oxidation behavior of the ITO surface.

By contrast, LiF deposited with reverse micelles (sol-LiF) has higher Φ than ITO, which also increases as a function of the coverage. For the sol-LiF monolayer, which by necessity has been subjected to O₂ plasma etching, Φ is larger than both Φ of the thermo-LiF/ITO, as

well as Φ of the etched (bare) ITO. The sub-monolayer (14.1% coverage) of sol-LiF/ITO revealed a measured work function of 5.29 ± 0.02 eV. In comparison with the 5.1 eV of PEDOT:PSS, the upper valence band edge of sol-LiF is much closer to that of commonly used organic HTLs. The projected lower barrier for hole carrier extraction suggests that sol-LiF/ITO would be well-suited for an organic solar cell electrode, for which an Ohmic contact with typical polymer layers is highly desirable.^{36,37} In fact, this unexpected advantage of the sol-LiF/ITO is particularly noteworthy, because a high performance organic polymer, PCDTBT, currently the subject of keen technological interest, has a HOMO level at ~ 5.5 eV.³⁸

It is remarkable that a dielectric film of nominally the same chemistry could induce a change in Φ in the opposite direction on the same electrode. However, such a phenomenon has previously been associated with the degree of surface coverage by alkali atoms on single crystal semiconductor substrates.³⁹ The adsorption of an isolated alkali atom induces a surface dipole moment, μ_0 , giving rise to a local change in the measured Φ . With increasing surface coverage, the onset of depolarization from the surrounding neighbor dipoles would diminish μ_0 , until a complete monolayer is formed. For surface coverage greater than a monolayer, the formation of a second alkali layer has given rise to a substantially different μ_0 , and consequent change in the globally measured Φ .

Most models of ultra-thin dielectric films on metal substrates assume continuous films fully wetting the surface. In such a case, two primary mechanisms have been proposed to explain the modification of the surface work function in opposite directions, determined in large part by the ionicity of the dielectric film.¹⁸ In the case of a positive change in Φ ($\Delta\Phi = |\Phi_{m/d} - \Phi_m| > 0$), an ultra-thin dielectric film would receive transferred charge from the metal. However, in the case of a dielectric film with highly ionic character, such as LiF, the effective work function would be lowered due to the electrostatic compression of the overspill electron density by the dielectric, also commonly referred to as the “pillow effect” ($\Delta\Phi = |\Phi_{m/d} - \Phi_m| <$

0). Although an oxide, ITO does have a high free charge carrier density, such that one could expect the formation of a surface dipole that would define the Φ of the bare ITO.

When the overspill charge encounters LiF, compression of the most energetic free electrons back into the ITO would lead to a negative change in Φ , which is typically observed in thermal evaporated LiF on metals. This electrostatic compression effect is commonly observed for physisorption and is well described in experimental and theoretical studies of self-assembled monolayer-modified metal work function.²⁰

In contrast, the formation of a sol-LiF/ITO bilayer induces the overspill of the ITO surface electron density beyond the ITO surface, manifested by an increase in the bilayer Φ . It is possible that the sol-LiF chemistry may not be pure, stoichiometric LiF, due to the necessary oxygen plasma etch. Indeed, the charged ionic particle surface may be a modified oxide, supported by the 0.3 eV charge-transfer shift observed for micelles in XPS (see Table 1 and Figure 3); in such a case, the difference in surface charge state may induce a stronger dipole moment and one of opposite polarity that draws electron density into the LiF layer, rather than compressing it, similar to the role that SAMs have played in increasing the work function of a metal electrode.²⁰

However, another possible scenario may be suggested by the increase in Φ with increasing surface coverage, as shown in Table 2. Deposition of sol-LiF on the ITO surface necessitates the gradual build-up of a layer of initially isolated LiF particles. Each individual LiF island corresponds to an isolated interface dipole. The formation of a surface dipole, in which electron density distribution is transferred away from the substrate surface, is susceptible to a depolarizing electric field arising from neighboring dipoles.⁴⁰ The surrounding dipole density may thus be the key.

Theoretical studies of the polarizability of an assembling monolayer of LiF revealed that the lateral polarizability gradually approaches that of the complete monolayer.⁴¹ Such a model suggests that as the surface density of LiF particles increases, the decreasing proximity

between neighboring particles perturbs the effective dielectric response surrounding each particle and leads to depolarization of the isolated dipole, as described in a sequence of schematics in Figure 4.

As proposed in a simplistic model by Langmuir for alkali adatoms on a metal substrate,⁴⁰ the mobile charge carriers in ITO can be approximated as a jellium of electron density (Figure 4a). When sol-LiF is brought into contact with the ITO, the ensuing polarization would draw the electron density distribution away from the ITO surface, and the dipole moment due to the LiF particles would contribute to a global increase in the bilayer surface work function (Figure 4b). With increasing coverage, a further increase would be induced in the surface work function,⁴² which was observed for LiF in the case of increasing from 14.1% to 29.3% coverage.

However, above a certain coverage, reduced interparticle separation enables neighboring electrical dipoles to depolarize, *i.e.* reducing the surface normal dipole moment and mitigating the magnitude of electron density transfer away from the ITO (Figure 4c). For a complete layer, the depolarization completely suppresses the initial charge transfer, and the observed surface work function can be described by the pillow-effect. This explanation is consistent with the both the increasing work function of sol-LiF and the subsequent observed decrease in work function for thermo-LiF/ITO bilayers, which have islands much broader than they are high, and eventually form a complete film. Clearly these results call for a deeper theoretical study on adsorbed discrete clusters of atoms on a metallic surface.

Finally, although $\Delta\Phi > 0$ is consistent with the O₂ plasma-treatment effect on ITO, which can be attributed to the adsorption of OH⁻ species on the surface,¹⁵ the increase in Φ cannot be solely attributed to oxidation. Firstly, the ITO substrates were exposed to toluene and ambient conditions between etching steps, which may reverse the improvement in work function with etching.⁴³ Secondly, increasing the O₂ plasma etching time has no effect on the Φ of ITO measured by SKP,¹⁵ therefore multiple plasma etching events should not lead to greater

oxidation nor a higher measured work function. It can only be attributed to the increase in the number of LiF islands (from $4.88 \times 10^{14} \text{ m}^{-2}$ to $1.20 \times 10^{15} \text{ m}^{-2}$), and hence greater charge transfer from the substrate on average.

We have shown that LiF produced from solution can be used to tune the surface work function of commonly used ITO electrodes in organic electronics. While the use of a solution-based ambient approach is itself attractive for the production of low cost organic devices, the ability to tune the surface work function using a controlled bottom-up approach is also of considerable interest in tailoring device performance, by customizing the energy level alignment for the specific electrode-organic interface of interest.

The use of reverse diblock copolymer micelles proved to be advantageous on two accounts. First, the polymeric micelles were used as nanoscale reactor vessels for the synthesis of LiF particles, circumventing the polydispersity problem. Second, they enabled the deposition of a 2-D array of LiF particles on the electrode surface with a controllable, ***uniform coverage***. Successive coating of layers enabled variation in the degree of sub-monolayer coverage of the LiF layer.

As the quest for higher efficiency also includes modifying the molecular orbital levels of the donor molecules to increase the open circuit voltage and wavelength absorption maxima, a controlled tunable surface work function would give a considerable advantage in the production of advanced solar cells. Our results suggest a correlation between Φ and LiF nanoparticle density, and currently work is in progress to substantiate this trend and elucidate the influence of this parameter on Φ .

SUPPORTING INFORMATION. DLS particle size distribution curves, work function maps, transmissivity curves, sheet resistance characteristics, and experimental details for

thermal evaporated LiF. This material is available free of charge via the Internet at <http://pubs.acs.org>.

ACKNOWLEDGEMENT Dr. S. Sturm and Dr. M. Ceh are acknowledged for TEM access at the Jozef Stefan Institute. At MPI-IS, F. Maye is acknowledged for experimental support, M. Weiland and Dr. L.P.H. Jeurgens for XPS measurements, Prof. J. Spatz for access to the SEM and plasma etcher, Dr. U. Welzel for x-ray diffraction measurements, and Dr. B. Mbenkum for experimental support with micelle reactors. D. C. Onduygu and G. Ersan are acknowledged for graphics design support. Dr. O. Gurlu is acknowledged for assistance in metallization. T.A. acknowledges a BIDEB 2210 scholarship from TÜBİTAK. A.T. acknowledges support by a Marie Curie International Incoming Fellowship and Reintegration Grant within the 7th European Community Framework Programme. Partial funding was provided by TÜBİTAK Grant #110T023.

REFERENCES

- (1) F.C. Krebs, *Sol. Energy Mater. Sol. Cells* **2009**, 93, 394;
- (2) F.C. Krebs, S.A. Gevorgyan, J. Alstrup, *J. Mater. Chem.* **2009**, 19, 5442-5451;
- (3) F.C. Krebs, T. Tromholt, M. Jorgensen, *Nanoscale* **2010**, 2, 873-886;
- (4) S.A. Gevorgyan, A.J. Medford, E. Bundgaard, S.B. Sapkota, H.-F. Schleiermacher, B. Zimmermann, U. Wuerfel, A. Chafiq, M. Lira-Cantu, T. Swonke, M. Wagner, C.J. Brabec, O. Haillant, E. Voroshazi, T. Aernouts, R. Steim, J.A. Hauch, A. Elschner, M. Pannone, M. Xiao, A. Langzettel, D. Laird, M.T. Lloyd, T. Rath, E. Maierm, G. Trimmel, M. Hermenau, T. Menke, K. Leo, R. Roesch, M. Seeland, H. Hoppe, T.J. Nagle, K.B. Burke, C.J. Fell, D. Vak, T.B. Singh, S.E. Watkins, Y. Galagan, A. Manor, E.A. Katz, T. Kim, K. Kim, P.M.

Sommeling, W.J.H. Verhees, S.C. Veenstra, M. Riede, M.G. Christoforo, T. Currier, V. Shrotriya, G. Schwartz, F.C. Krebs, *Sol. Energy Mater. Sol. Cells* **2011**, 95, 1398-1416.

(5) C. Lungenschmied, G. Dennler, H. Neugebauer, S.N. Sariciftci, M. Glatthaar, T. Meyer, A. Meyer, *Sol. Energy Mater. Sol. Cells* **2007**, 91, 379.

(6) G. Li, V. Shrotriya, J.S. Huang, Y. Yao, T. Moriarty, K. Emery, Y. Yang, *Nat. Mater.* **2005**, 4, 864.

(7) J.M. Zhao, S.T. Zhang, X.J. Wang, Y. Q. Zhan, X.Z. Wang, G. Y. Zhong, Z.J. Wang, X.M. Ding, W. Huang, X.Y. Hou, *Appl. Phys. Lett.* **2004**, 84, 2913.

(8) Y. Zhao, S. Y. Liu, J.Y. Hou, *Thin Solid Films* **2001**, 397, 208.

(9) F.R. Zhu, B.L. Low, K.R. Zhang, S.J. Chua, *Appl. Phys. Lett.* **2001**, 79, 1205.

(10) C.J. Brabec, S.E. Shaheen, C. Winder, N.S. Sariciftci, P. Denk, *Appl. Phys. Lett.* **2002**, 80, 1288.

(11) D. Grozea, A. Turak, X.D. Feng, Z.H. Lu, D. Johnson, R. Wood, *Appl. Phys. Lett.* **2002**, 81, 3173.

(12) L.S. Hung, C.W. Tang, M.G. Mason, *Appl. Phys. Lett.* **1997**, 70, 152.

(13) R. Schlaf, B.A. Parkinson, P.A. Lee, K.W. Nebesny, G. Jabbour, B. Kippelen, N. Peyghambarian, N.R. Armstrong, *J. Appl. Phys.* **1998**, 84, 6729.

(14) C.C. Wu, C.I. Wu, J.C. Sturm, A. Kahn, *Appl. Phys. Lett.* **1997**, 70, 1348.

(15) J.S. Kim, B. Lagel, E. Moons, N. Johansson, I.D. Baikie, W.R. Salaneck, R.H. Friend, F. Cacialli, *Synth. Met.* **2000**, 111, 311.

(16) E. Ahlswede, J. Hanisch, M. Powalla, *Appl. Phys. Lett.* **2007**, 90, 163504.

(17) M. Reinhard, J. Hanisch, Z. Zhang, E. Ahlswede, A. Colsmann, U. Lemmer, *Appl. Phys. Lett.* **2011**, 98, 053303.

(18) S. Prada, U. Martinez, G. Pacchioni, *Phys. Rev. B* **2008**, 78, 235423.

(19) N. Koch, A. Kahn, J. Ghijsen, J.J. Pireaux, J. Schwartz, R.L. Johnson, A. Elschner, *Appl. Phys. Lett.* **2003**, 82, 70.

(20) G. Heimel, L. Romaner, E. Zojer, J.-L. Bredas, *Acc. Chem. Res.* **2008**, 41, 721.

(21) A. Sharma, B. Kippelen, P.J. Hotchkiss, S.R. Marder, *Appl. Phys. Lett.* **2008**, 93, 163308.

(22) D.J. Milliron, I.G. Hill, C. Shen, A. Kahn, J. Schwartz, *J. Appl. Phys.* **2000**, 87, 572.

(23) S. Forster, M. Antonietti, *Adv. Mater.* **1998**, 10, 195.

(24) O. El-Atwani, T. Aytun, O.F. Mutaf, V. Srot, P.A. van Aken, C.W. Ow-Yang, *Langmuir* **2010**, 26, 7431.

(22) Polystyrene₄₆₆-*b*-poly 2vinyl pyridine₆₆₆ (PDI = 1.08) was dissolved in toluene (3 mg mL⁻¹) under vigorous stirring for 24 hours. Non-hydrated lithium hydroxide (0.6 mg mL⁻¹, Merck) was added, then stirred vigorously for 4 days. Undissolved LiOH was removed by centrifuging at 4500 rpm for 30 minutes. DLS showed an average micelle size increase from 16.7 nm to 67 nm. HF (0.56 mL L⁻¹, Merck technical grade) was added, then stirred continuously for 24 hours. Spin-coating was performed using 2000 rpm for 40 s onto silicon wafer and bare ITO-coated glass (TFD Ltd, 30 ohm □⁻¹) substrates. Oxygen plasma etching was performed using optimized parameters (PVA Tepla America Inc., 150 W, 0.1 mbar O₂, 45 min.; and Harrick PDC-002, 29.6 W, 150 mTorr, 60 min.). TEM: JEOL 2010F, operated at 200 keV, on loaded micelle samples drop-cast onto formvar-coated Cu grid supported lacey carbon; X-ray diffraction measurements (Panalytical X'Pert Pro Diffractometer): Cu-K_α

radiation (45 kV, 40 mA), parallel beam, 4 mm × 4 mm defined by crossed slits; loaded micelle samples drop-cast onto amorphous glass slides; XPS (ThetaProbe, Thermo VG Scientific): monochromatic Al K_α source, 15 μm spot size; SEM (Zeiss Supra 55 VP) operated at 1 keV. SKP measurements (KP Technology, SKP5050 Scanning Kelvin Probe) were performed using a 2-mm diameter probe head, off-null method, and tip-to-sample tracking within 1 micron; data sets were nearest neighbor fitted, to yield the average Φ value over the scanned surface. Thermal evaporated LiF (Omicron NanoTechnology GmbH): UHV (10⁻¹⁰ mbar), water-cooled Knudsen source, ~1 Å/min. deposition rate, 0.5 and 1 nm nominal thickness; prior to thermal evaporation, ITO substrates annealed at 130°C in vacuum, 30 min. See Supporting Information for more details.

(26) G. Kastle, H.G. Boyen, F. Weigl, G. Lengl, T. Herzog, P. Ziemann, S. Riethmuller, O. Mayer, C. Hartmann, J.P. Spatz, M. Moller, M. Ozawa, F. Banhart, M.G. Garnier, P. Oelhafen, *Adv. Funct. Mater.* **2003**, 13, 853.

(27) I.D. Baikie, P. J. Estrup, *Rev. Sci. Instrum.* **1998**, 69, 3902.

(28) R. Sarraf-Mamoory, S. Nadery, N. Riahi-Noori, *Chem. Eng. Commun.* **2007**, 194, 1022.

(29) D. Briggs, *Handbook X-ray and ultraviolet photoelectron spectroscopy*, Heyden & Son, Ltd., London, UK **1977**.

(30) J. Cazaux, *J. Electron Spectrosc. Relat. Phenom.* **1999**, 105, 155.

(31) C.Q. Sun, *Phys. Rev. B* **2004**, 69, 045105.

(32) B. Balamurugan, T. Maruyama, *Appl. Phys. Lett.* **2006**, 89, 033112.

(33) A.I. Kovalev, D.L. Wainstein, A.Y. Rashkovskiy, A. Osherov, Y. Golan, *Surf. Interface Anal.* **2010**, 42, 850.

- (34) Y.J. Lin, I.D. Baikie, W.Y. Chou, S.T. Lin, H.C. Chang, Y.M. Chen, W.F. Liu, *J. Vac. Sci. Technol. A* **2005**, 23, 1305.
- (35) H.S. Kim, H. Lee, P.E. Jeon, K. Jeong, J.H. Lee, Y. Yi, *J. Appl. Phys.* **2010**, 108, 053701.
- (36) M.C. Scharber, D. Muhlbacher, M. Koppe, P. Denk, C. Waldauf, A.J. Heeger, C.L. Brabec, *Adv. Mater.* **2006**, 18, 789.
- (37) T. Aytun, A. Turak, C.W. Ow-Yang, Sabanci University, Istanbul, Turkey. Unpublished work (Preliminary studies with P3HT:PCBM and small molecule devices reveal an increase in J_{sc}), 2011.
- (38) S.H. Park, A. Roy, S. Beaupre, S. Cho, N. Coates, J.S. Moon, D. Moses, M. Leclerc, K. Lee, A.J. Heeger, *Nat. Photonics* **2009**, 3, 297.
- (39) R.E. Weber, W.T. Peria, *Surf. Sci.* **1969**, 14, 13.
- (40) N.D. Lang, *Phys. Rev. B* **1971**, 4, 4234.
- (41) M. Ferrero, M. Rerat, R. Orlando, R. Dovesi, *J. Comput. Chem.* **2008**, 29, 1450.
- (42) D.M. Taylor, G. F. Bayes, *Phys. Rev. E* **1994**, 49, 1439.
- (43) Z.Z. You, J.Y. Dong, S.D. Fang, *Phys. Status Solidi A* **2004**, 201, 3221.

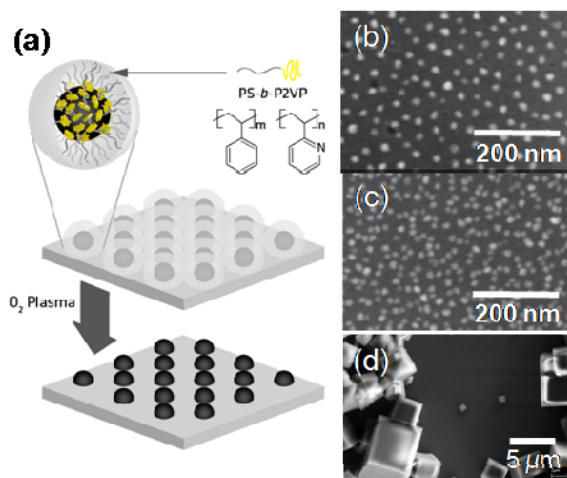


Figure 1. (a) Schematic illustration of the process for forming LiF nanoparticles in micelle nanoreactors, leading to deposition of a monolayer of LiF-containing micelles onto ITO by spin coating, and finally O₂ plasma etching to remove the polymer. Scanning electron microscope (SEM) images revealing the increase in sub-monolayer coverage of LiF formed in solution with the assistance of micelle reactors from (b) a single deposition of LiF, after etching with O₂ plasma; to (c) three times successively spin coating and O₂ plasma etching LiF—both images of the same magnification. To demonstrate the effect of micelle reactor processing, the SEM image of polydisperse crystals is shown in (d), for LiF formed in solution without the use of micelle reactors.

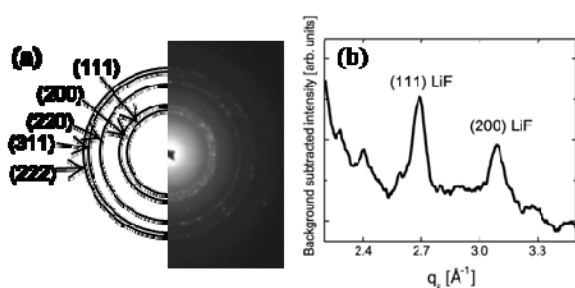


Figure 2. The formation of crystalline LiF in the polymeric micelles is validated by (a) electron diffraction and (b) background subtracted x-ray diffraction pattern.

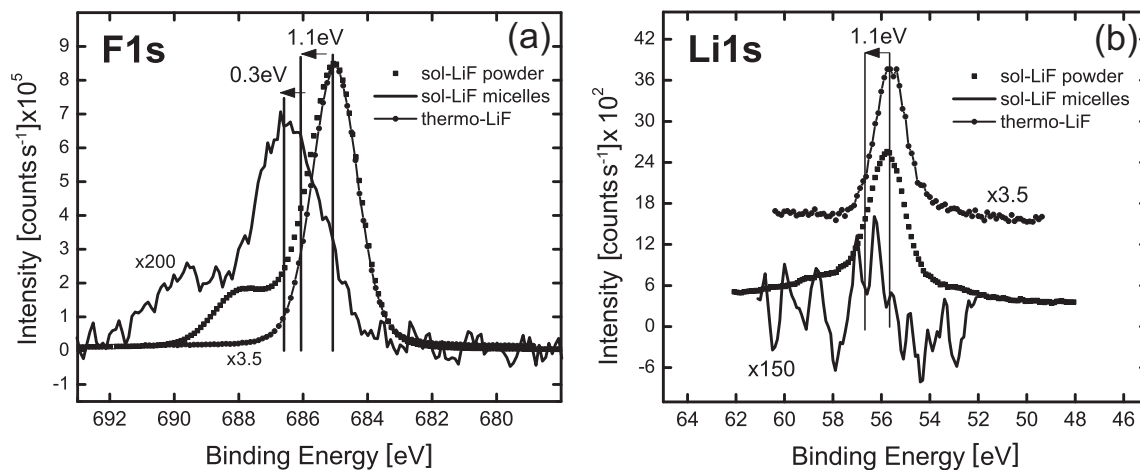


Figure 3. (a) F-1s and (b) Li-1s core levels from solution processed and thermally evaporated LiF. All spectra were aligned to adventitious C at 284.8 eV. The micelles exhibit both a 1.1 eV charging-shift due to non-uniform charging of the nanoparticles, and a 0.3 eV charging-shift in F-1s due to charge transfer from the substrate.

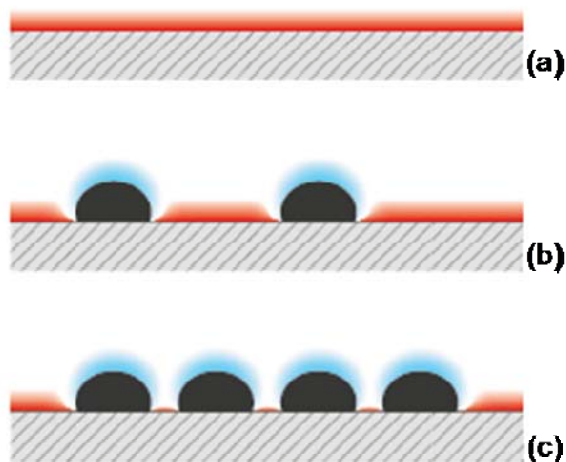


Figure 4. Cross-section view of the electron density distribution (in red) shown for (a) the substrate surface, and (b) isolated LiF particles on the substrate surface introducing an interfacial dipole moment (in blue). In (c) the interparticle spacing has been reduced, such that neighboring LiF dipoles interact; perturbation of the effective dielectric environment of a LiF particle leads to a reduction in the interfacial dipole moment.

Table 1. X-ray photoelectron spectroscopy parameters for solution processed and thermally evaporated LiF, showing the details from the main 1s core levels for Li and F

| Material | F-1s [eV] | Li-1s [eV] | $\Delta BE_{(F1s-Li1s)}$ | Concentration ratio (Li:F) |
|---------------------------|--------------|---------------|--------------------------|-------------------------------|
| sol-LiF micelle | 686.4 | 56.4 | 630 | 0.97 |
| sol-LiF powder | 685 | 55.3 | 629.7 | 0.88 |
| thermo- LiF (100 Å) | 686 | 56.6 | 629.4 | 0.90 |

Table 2. Summary of extracted work function (Φ) from SKP using a 2-mm calibrated polycrystalline Au tip (calibrated to Au surface with $\Phi = 5.10$ eV).

| Sample | Avg. Φ [eV] | $\Delta \Phi$ |
|----------------------------------|------------------|---------------|
| thermo-LiF, 0.5 nm thick | 5.06 ± 0.01 | -0.045^a |
| thermo-LiF, 0.5 nm thick, etched | 5.20 ± 0.02 | -0.034^a |
| thermo-LiF, 1 nm thick | 4.89 ± 0.06 | -0.167^a |
| sol-LiF, etched, 14.1% coverage | 5.29 ± 0.02 | 0.032^b |
| sol-LiF, etched, 29.3% coverage | 5.44 ± 0.03 | 0.189^b |
| Bare ITO, etch-treated | 5.25 ± 0.03 | 0.130^c |
| Bare ITO | 5.12 ± 0.06 | — |

^arelative to the ITO surface, masked during thermal evaporation

^brelative to the etched ITO surface

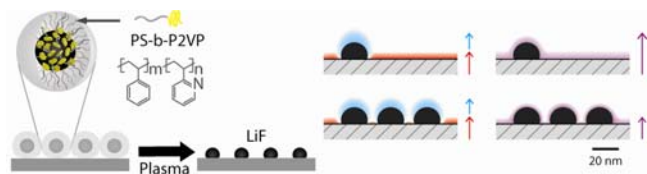
^crelative to the as-received ITO surface

The table of contents entry

Keyword: surface work function tuning, Kelvin probe, organic solar cells, LiF, depolarization, reverse diblock copolymer micelles

T. Aytun, A. Turak, I. Baikie, G. Halek, and C.W. Ow-Yang*

Solution-Processed LiF for Tailoring the Work Function in Electrode Bilayers



Tunability in the surface work function of ITO can be achieved by controlled deposition of isolated LiF nanoparticles synthesized inside reverse diblock copolymer micelles. By increasing the number of layers of loaded micelles, a well-defined build-up of the LiF interlayer is achieved, enabling control over the interfacial dipole contribution to the overall surface work function.

SUPPORTING INFORMATION

LiF Synthesized Inside Micelle Reactors

A monodisperse size distribution of the system, as shown by a single peak in Figure S1, verified the loading of the PS(48,500)-*b*-P2VP(70,000) reverse micelles, probed by dynamic light scattering (Zetasizer Nano, Malvern Instruments Ltd.). The presence of a salt incorporated into the micelle core stabilizes the PS-*b*-P2VP reverse micelle structures dissolved in toluene.^{1,2}

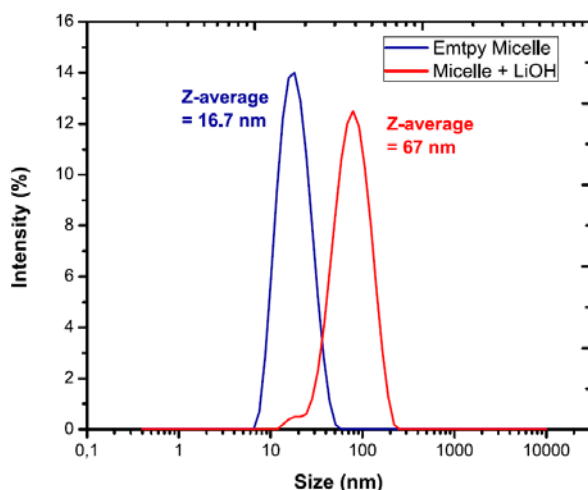


Figure S1. Dynamic light scattering result for empty and LiOH loaded micelles, average size increased from 16.7 nm to 67 nm upon loading of LiOH.

Etching parameters

To remove the polymeric micelle reactor and expose the LiF nanoparticles, plasma etching was performed (PVA Tepla America Inc. and Harrick PDC-002). Both H₂ and O₂ plasma sources were examined, under a variety of RF power, pressure, and time combinations to determine the optimal conditions. As N only exists in the P2VP unit of the micelle copolymer, the optimal conditions were established by monitoring the N1s signal by XPS (ThetaProbe, Thermo VG Scientific, Al K_α source). Various processing conditions are shown in Figure S2,

with O₂ etching showing better polymer removal characteristics than H₂. Based on these results, the etching conditions were set at 150 W, 0.1 mbar O₂, 45 min or 29.6 W, 150 mTorr, 60 min, depending on the plasma etcher used.

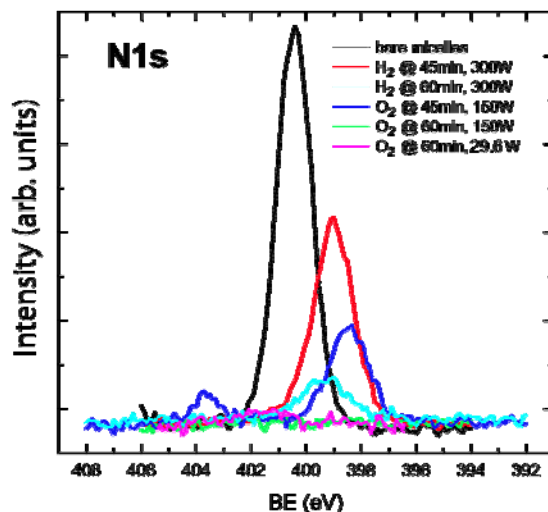


Figure S2. XPS N1s core level for various plasma etching conditions

Work Function Maps

The work function of LiF deposited onto ITO was mapped by scanning Kelvin Probe (SKP5050, KP Technology), and the maps are shown in Figure S3. The macroscopic Kelvin probe tip was calibrated on a pristine (freshly evaporated) gold surface—33-nm thick, deposited on aluminum. This surface is routinely used as a calibration surface. The value was measured in air, under controlled Relative Humidity (RH) conditions, typically 40-42% RH and 293 K. The samples were measured under identical conditions.

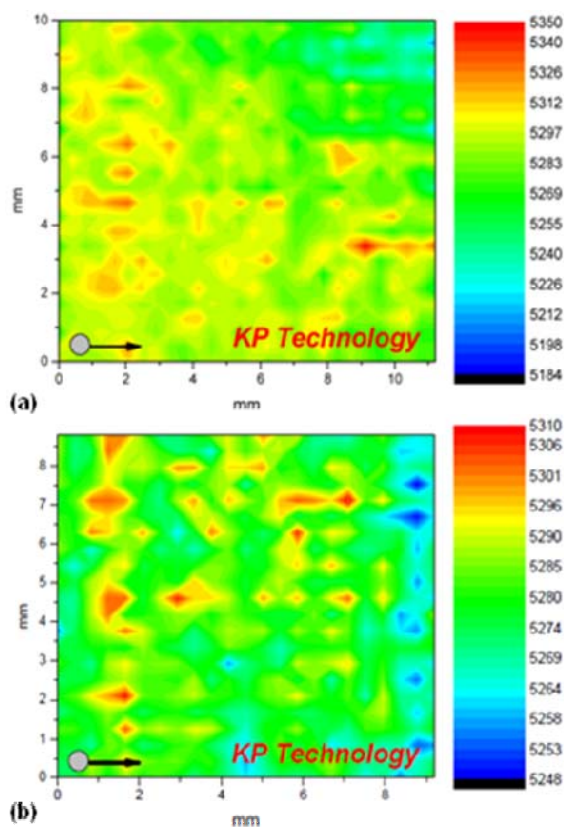


Figure S3. Maps of the surface work function as measured by scanning Kelvin probe for (a) a single deposition of LiF, after etching with O₂ plasma; and for (b) three times successively spin coating and O₂ plasma etching LiF. Note that the apparent regular pattern of high Φ at 2 mm is uncorrelated with the pattern of LiF nanoparticle dispersion on the surface.

Transmittance

For use in solar cell devices, the transparent electrode should have as high optical transmission in the visible region as possible. To assess the transmissivity of the LiF-coated electrode surfaces, optical transmission measurements were performed under ambient conditions from 200-800 nm, relative to the incident probe illumination as the reference in a UV-visible spectrophotometer (UV-3150, Shimadzu). Figure S4 and Table S1 summarize the results. As LiF has high optical transparency from UV to extreme IR,³ the transmissivity of

the LiF nanoparticle-coated ITO showed little attenuation at all wavelengths. Some enhancement was even observed for higher coverage (29.3%) of LiF nanoparticles, which suggests that the apparent attenuation at lower coverage (14.1%) can be attributed to differences in the underlying ITO or to scattering effects on the rough surface. The change in the spectrum shape below 400 nm is likely a function of LiF absorption at those wavelengths.³ All values of transmittance within 2.5% of that of ITO at all wavelengths, and are well within the range of ITO used in solar cells.⁴

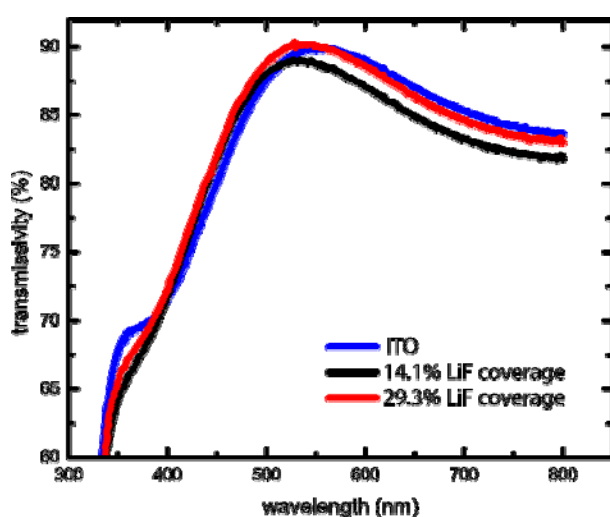


Figure S4. Optical transmittance for bare and coated ITO surfaces over visible wavelengths.

Table S1. Transmittance values for bare and coated ITO surfaces

| | peak max [nm] | T% @peak max | %diff | T% @700nm | %diff | T% @400nm | %diff |
|-----------|---------------------|-----------------|--------|--------------|--------|--------------|-------|
| ITO | 544.0 | 89.94 | 0.00% | 85.28 | 0.00% | 71.66 | 0.00% |
| 14.1% LiF | 528.5 | 89.04 | -1.00% | 83.27 | -2.36% | 71.93 | 0.37% |
| 29.3% LiF | 528.5 | 90.33 | 0.44% | 84.64 | -0.75% | 72.35 | 0.95% |

Sheet Resistance

The sheet resistance of the ITO films with and without the LiF particles was measured by 4-point probe, with the deviations from bare ITO summarized in Table S2. The pogo-pin probe tips (Interconnect Devices, Inc.) were ~0.5 mm in diameter, contacting areas of the sample surface that would encompass the influence of many LiF nanoparticles. Because the difference in sheet resistance for the LiF-coated samples was below the 20% error quoted by the manufacturer, it can be concluded that the LiF particle surface coverage is of too low a density to impact the sheet resistance of the ITO.

Table S2. Change in sheet resistance values for coated ITO surfaces

| Sample | Deviation from bare ITO | % difference |
|-----------|-------------------------|--------------|
| ITO | 0 | -- |
| 14.1% LiF | -0.00769 | -6% |
| 29.3% LiF | -0.00499 | -4% |

Thermally evaporated LiF

For comparison, thermal evaporation of LiF powder was performed under ultra-high vacuum (10^{-10} mbar) conditions in a commercial UHV system (Omicron NanoTechnology GmbH) from a water-cooled Knudsen source. Using a deposition rate of ~1 Å/min., LiF films were deposited with nominal thickness of 0.5 and 1 nm, as monitored by a quartz crystal microbalance (QCM). Prior to thermal evaporation, the ITO substrates were annealed at 130°C in vacuum for 30 min. to remove absorbed water and contaminants. During thermal evaporation of LiF, the ITO substrate was masked, to produce regions of LiF covered ITO, and bare ITO for direct comparison with the Kelvin probe, as shown in Figure S5. Atomic force microscopy measurements were done in air using a Veeco Digital Instruments CP-II SPM system in tapping mode. The non-contact silicon tips were MPP-11123-10 (Veeco) with

a resonance frequency of 285-327 kHz, and a force constant of 20-80 N/m. The AFM images were processed with the free software WSxM (NanoTec).⁵ X-ray diffraction measurements were performed in a Philips (now Panalytical) X'Pert Pro Diffractometer, with a parallel beam formed by an X-ray lens in the primary beam and parallel-plate collimator in the diffracted beam, beam size set to 4 mm × 4 mm by crossed slits, Cu-K α radiation from a sealed X-ray tube (45 kV, 40 mA). Thermally evaporated LiF on ITO is polycrystalline, with nearly the $\langle 522 \rangle$ texture expected for LiF thin films on amorphous substrates.⁶

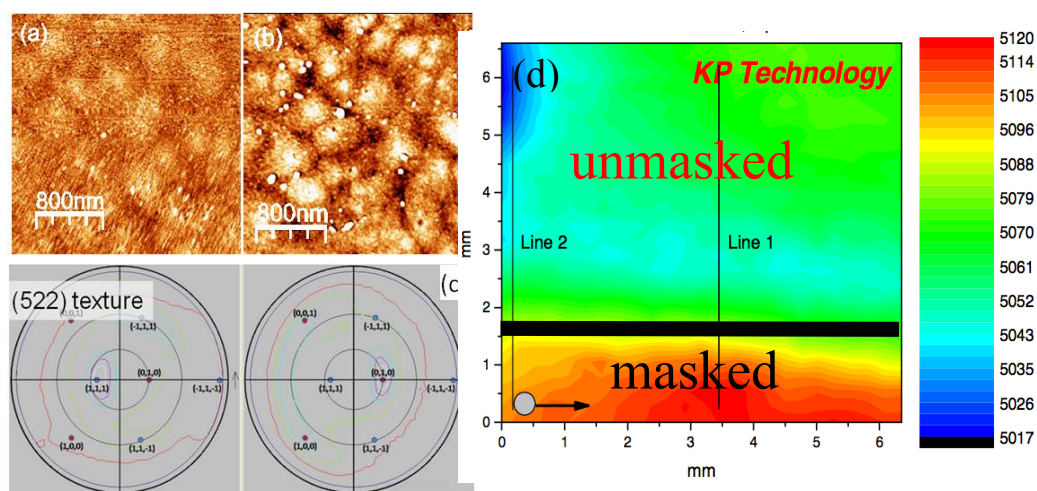


Figure S5. (a) MPI3: 10Å LiF thermally evaporated on ITO (b) masked region of MPI3 showing the ITO surface. (non-contact AFM) (c) Overlay of stereographic projection for LiF with indication of the 100 and 111 poles and the measured pole figures for the 111 (left) and 200 (right) reflections of thermally evaporated LiF (1000Å) on ITO. The pole figures show a texture approaching that of the $\langle 522 \rangle$ expected for LiF thin films without epitaxial matching. (d) Work function map of the ITO surface showing the masked and unmasked regions, and corresponding work function.

For comparison, LiF was also thermally evaporated onto an organic thin film surface as shown in Figure S6. Diindenoperylene (DIP) was acquired from the University of Stuttgart,

and purified twice by gradient sublimation before use. The deposition was performed by thermal evaporation from home built Knudsen cells with a deposition rate of approximately 0.2 monolayer (ML) per minute for the organic and 1 Å per minute for LiF, determined with a calibrated quartz crystal monitor (QCM). The substrate temperature during growth was controlled by a resistive heater, with temperature oscillation less than 1°. Note the appearance of hemispherical islands 0.5-1 nm in diameter (which appear larger in atomic force microscope (AFM) images due to tip-surface convolution).

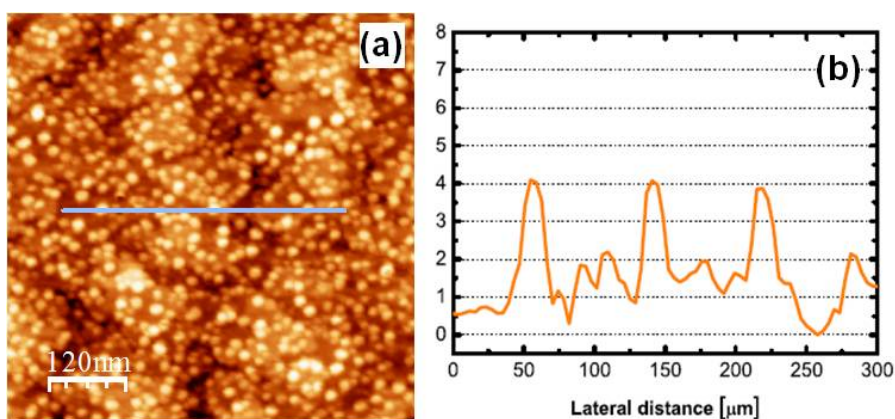


Figure S6. (a) Thermally evaporated LiF (5 Å by QCM) on diindenoperylene (5ML) (non-contact AFM) (b) corresponding height profile

- (1) J. Q. Lu, *J. Phys. Chem. C* **2008**, 112, 10344-10351.
- (2) O. El-Atwani, T. Aytun, O.F. Mutaf, V. Srot, P.A. van Aken, C.W. Ow-Yang, *Langmuir* **2010**, 26, 7431-7436.
- (3) D.B. Sirdeshmukh, L. Sirdeshmukh, K. G. Subhadra, *Alkali Halides: A handbook of physical properties*; Springer: Berlin, Germany, 2001; p. 122..
- (4) H.B. Saim, D.S. Campbell, J.A. Avaritsiotis, *Solar Energy Materials* **1986**, 13, 85-96.

(5) I. Horcas, R. Fernandez, J. M. Gomez-Rodriguez, J. Colchero, J. Gomez-Herrero, A.M. Baro, *Rev. Sci. Instrum.* **2007**, 78, 013705.

(6) P. E. Di Nunzio, L. Fornarini, S. Martelli, R.M. Montereali, *Phys. Status Solidi A* **1997**, 164, 747-756.